Fatigue Crack Propagation in Mode II and Sequential Mode I-II in Ferritic-Pearlitic Steel

V. Doquet[1] and S. Pommier[2]
[1] LMS. Ecole Polytechnique. 91128 Palaiseau cedex. France
doquet@lms.polytechnique.fr
[2] LMSS-MAT. Ecole Centrale. Grande voie des Vignes. 92295 Chatenay Malabry
sylvie@mssmat.ecp.fr

ABSTRACT. *Mode II fatigue crack growth tests as well as tests in sequential Mode I then Mode II were performed on ferritic-pearlitic steel. For ΔK_{II} ranging from 7 to 43MPa$\sqrt{m}$, bifurcation occurs after 12 to 450 μm coplanar growth, at a decreasing speed. By contrast, hundreds of microns of constant speed coplanar growth were obtained under sequential Mode I then Mode II loading, for ΔK_{II} = 20MPa$\sqrt{m}$ and ΔK_I ranging from 0.25 to 1.0 ΔK_{II}. The crack growth rate is a simple sum of the contributions of each mode for ΔK_I equal to 0.25ΔK_{II} but above this value, a synergetic effect is found. The mechanism of this fast propagation mode is discussed in the light of strain range maps ahead of the crack tip obtained by digital SEM images correlation and elastic-plastic finite elements calculations. The stability of the crack path according to the maximum growth rate criterion is demonstrated.*

INTRODUCTION

Surface initiated cracks in rolling contact fatigue of rails, wheels, bearing or gears are often submitted to a complex sequence of Mode I + II loading, but few studies have yet been devoted to crack growth under such non-proportional loadings. Wong et al.[1] observed fast and stable coplanar growth when Mode I and II were applied sequentially and proposed empirical equations combining ΔK_I and ΔK_{II} to correlate kinetic data. The aim of the present study is to improve the understanding of the local mechanisms of such propagation modes through accurate measurements and analysis of crack tip plastic strain and displacement fields during tests performed in a SEM.

MATERIAL, EXPERIMENTAL AND NUMERICAL PROCEDURES

Steel for railway applications ($R_{p(0,2)}$ = 567MPa, Rm = 898MPa) was studied. The microstructure consists of 30μm wide equiaxial pearlite and ferrite grains.

Precracked tubular specimens (10.8 and 9mm external/internal diameters) and 3mm thick CTS specimens covered with microgrids with a 4 μm pitch were used.

Mode II crack propagation tests were carried out at 0.5 Hz with K_{min}/K_{max} equal to zero for CTS specimens and -1 for tubular specimens. Tests were also performed under

sequential Mode I (R=0) then Mode II (R=-1) loading, at 0.1Hz, on pre-cracked tubular specimens successively loaded in tension and reversed torsion.

CTS or tubular specimens were periodically transferred to a tension/torsion loading frame inside a S.E.M. Crack flanks relative displacements were then measured at both K_{min} and K_{max} using microgrids as reference marks. During sequential mixed mode tests, correlation of high resolution digital images of the crack tip area taken during a cycle, at K_{Imin} and K_{Imax} or K_{IImin} and K_{IImax}, respectively, yield the relative displacement field and by derivation, maps of local strain ranges associated with each loading mode.

Finite element analyses have also been conducted using Abaqus in order to distinguish the role of plasticity from that of crack flanks friction. A crack in a large rectangular plate with prescribed shear stress along the four sides was modelled. Quadratic triangular elements and plane stress conditions were employed. The mesh size at crack tip was 0.25 μm. An elastic-plastic constitutive equation with non-linear kinematic hardening fitted to the stress-strain curves of the material was used.

RESULTS

Mode II

Coplanar crack growth was observed over a distance increasing from 12 to 450μm for nominal ΔK_{II} ranging from 7 to 43 MPa$\sqrt{m}$ (Fig. 1a). The Mode II kinetic data are plotted on Fig. 1b as a function of effective S.I.Fs (in spite of some restrictions, below).

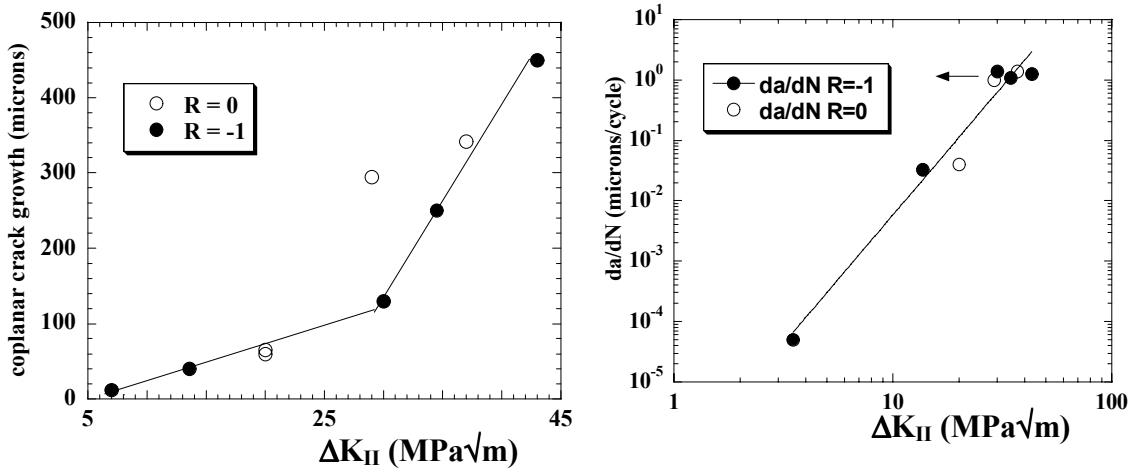

Figure 1. Synthesis of Mode II data.

For ΔK_{II}=7MPa$\sqrt{m}$ and R=-1, the analysis of measured crack flanks relative displacements (Fig. 2a) yields an effective ΔK_{II} of 3.5 MPa$\sqrt{m}$. Shielding by friction is thus rather important for this loading range. For 13.7 MPa$\sqrt{m}$ (Fig. 2b) and R=-1, the measured displacements fall between the asymptotic elastic sliding displacements and the elastic-plastic values computed by FEM, over the first 250μm. It seems thus reasonable to assume that $\Delta K_{II}^{effective}$ =13.7MPa$\sqrt{m}$. For 43MPa$\sqrt{m}$ and R=-1, the

experimental points superpose onto the theoretical elastic asymptotic profile but are well below the elastic-plastic profile. $\Delta K_{II}^{effective}$ was thus less than 43MPa$\sqrt{m}$ but it is difficult to specify its value (whence the arrow on Fig. 1b).

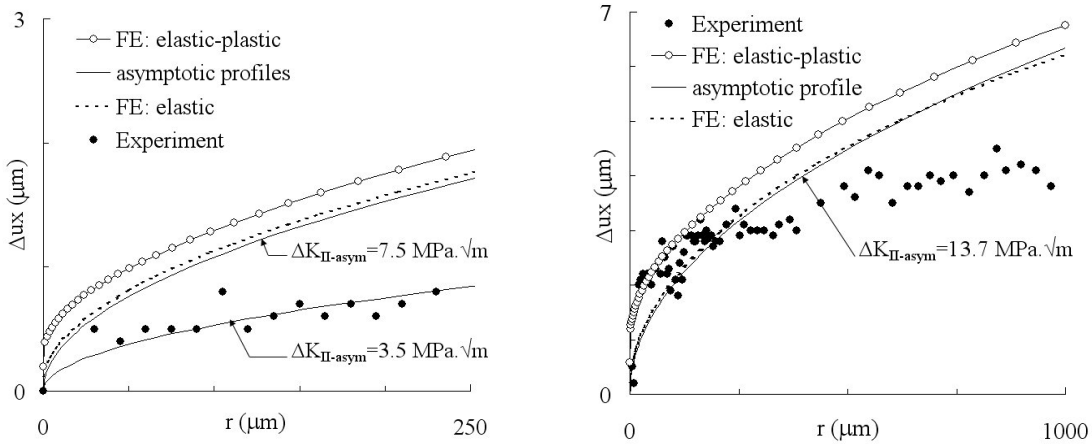

Figure 2. Sliding displacement profiles for ΔK_{II}=7 (left) and 13.6MPa$\sqrt{m}$ (right), R=-1.

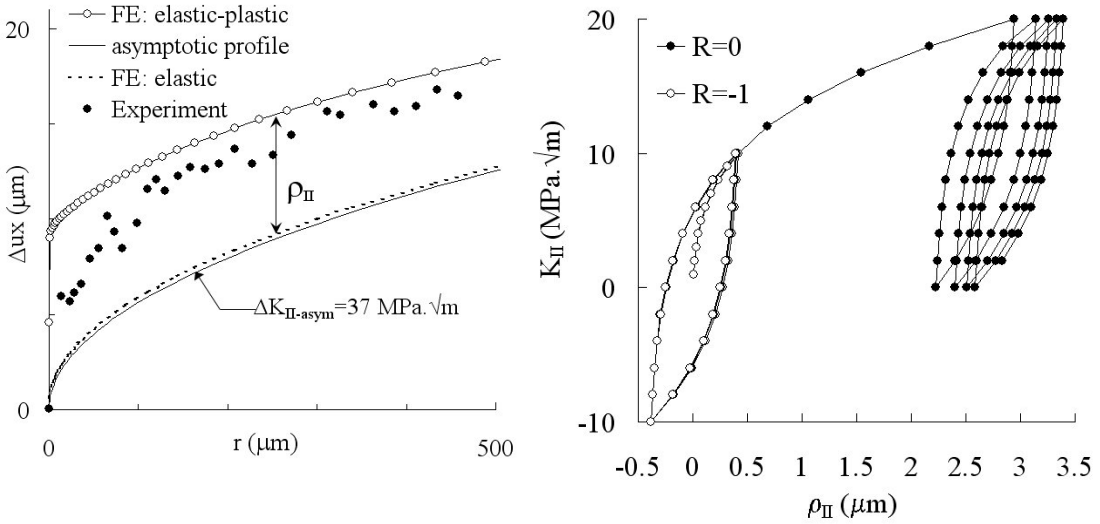

Figure 3. a) Sliding displacement profiles for ΔK_{II}=37MPa$\sqrt{m}$, R=0. b) Evolution of the "plastic sliding displacement" ρ_{II}, for ΔK_{II}=20MPa$\sqrt{m}$, 250 μm behind the crack tip.

For ΔK_{II}=29 and 37 MPa$\sqrt{m}$ and R=0 (for which K_{IImax} were higher than for R=-1, but maximum applied shear stresses lower than 38% of the 0.2% shear yield stress), the measured displacement profiles were above that predicted by LEFM (Fig. 3a) but anyway still below the "elastic-plastic" profile. The difference between measured and computed elastic-plastic profiles, which can be attributed to friction on the crack flanks

diminishes when ΔK_{II} increases (compare Fig. 2 and Fig. 3), consistently with the literature. A rigourous method to derive $\Delta K_{II}^{effective}$ when crack tip plasticity is consequent has to be settled.

It was noticed that for R=0, wear of the asperities was faster than during reversed loading, as suggested by the higher flow of debris exuding from the crack flanks. Ratchetting in the crack flanks sliding displacement was also more pronounced as evidenced by the important residual shift of the microgrids at zero load, after only 200 cycles at 37 MPa$\sqrt{m}$, on Fig. 4. This effect was confirmed using the FEM as shown by Fig. 3b on which the difference (ρ_{II}) between the elastic and the elasto-plastic sliding displacement is plotted. For a given value of ΔK_{II}, cyclic plasticity is similar at R=-1 and at R=0, though ratchetting appears at R=0 and not at R=-1. The absence in the experimental results of a clear influence of the R ratio on the crack growth rates (within the limited data yet available) may thus seem surprising.

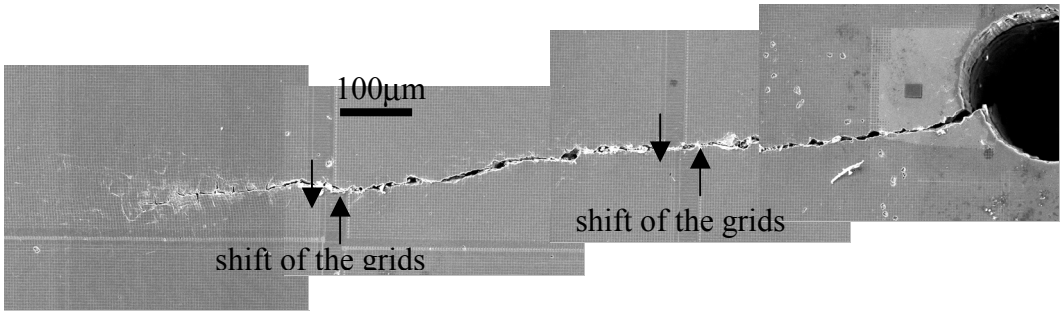

Figure 4. Aspect of a crack at zero load, after 200cycles at 37 MPa$\sqrt{m}$, R=0.

Sequential Mode I-II

Figure 5a shows the evolution of the half crack length measured during a test under sequential Mode I +II, with ΔK_{II}=20MPa$\sqrt{m}$ and ΔK_I initially equal to ΔK_{II}, later reduced to $0.75\Delta K_{II}$, then $0.5\Delta K_{II}$, then $0.25\Delta K_{II}$ and finally zero (the latter condition leading to immediate bifurcation). Compared to what is observed in pure Mode II, the quantity of fretting debris rejected by the flanks is limited and no deceleration appears when the crack propagates over several hundreds of microns, under constant nominal ΔK_{II}, which suggests an attenuation of friction forces.

Since there is no deceleration, a unique growth rate can be defined for each mode mixity ratio. Figure 5b shows that the growth rate increases regularly with ΔK_I up to $0.75\Delta K_{II}$ but that beyond this value, the increase is suddenly more rapid. Open symbols correspond to a simple sum of the Mode I and Mode II growth rates for the corresponding S.I.Fs. The measured growth rates are clearly higher than these estimates (a factor of three higher when ΔK_I reaches ΔK_{II}), which means that a synergetic effect is present.

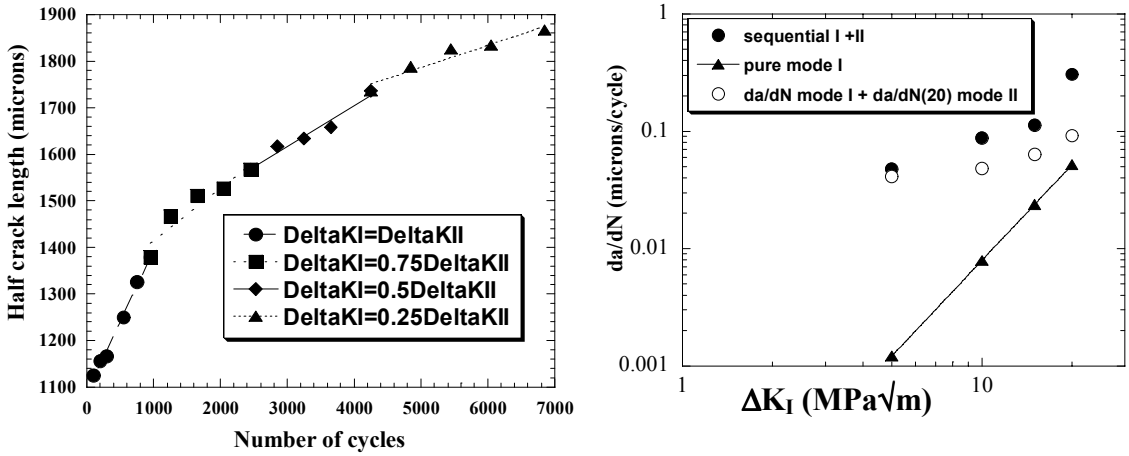

Figure 5. Kinetic data for sequential Mode I –II.

As concerns the aspect of the crack developed during this test, the roughness as well as the number and length of aborted branches increase as ΔK_I decreases, but the average direction of propagation however remains unchanged (Fig. 6).

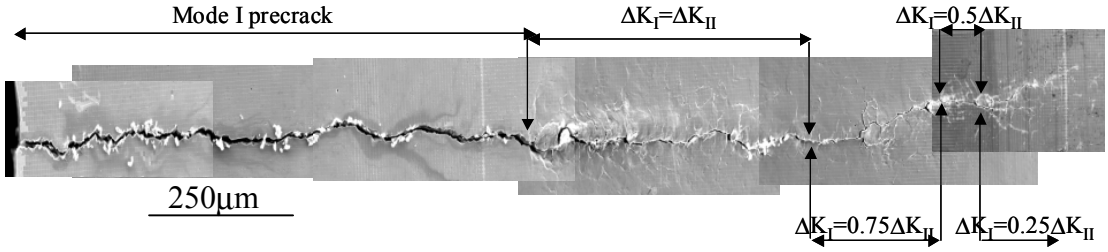

Figure 6. One side of the crack formed under sequential Mode I – II.

Figure 7 shows the shear and tensile strain range profiles measured ahead of the crack tip during the Mode II stage of the cycle, for $\Delta K_I = \Delta K_{II}$. It can be observed that large tensile plastic strains are produced by the Mode II cycle along a line theoretically loaded in pure shear (and conversely, large shear strains are measured along the ligament during the Mode I part of a cycle). This coupling is less pronounced when ΔK_I is equal to $0.75\Delta K_{II}$. That is why it is not suspected to be due to some asperity induced opening of the crack, which has no reason to decrease in those cases where, at the contrary, roughness increases. Furthermore, the plastic flow in shear measured along the ligament during the tensile part of the cycle cannot be attributed to some Mode II component since the corresponding images of the crack flanks do not suggest any sliding displacement.

The sliding displacement range profiles measured during the Mode II part of a cycle, (open or filled symbols for each crack tip) are plotted on Fig. 8a for the first three parts of the test. The measured displacements are well above the LEFM asymptotic profile and even above the elastic-plastic profile computed for pure Mode II.

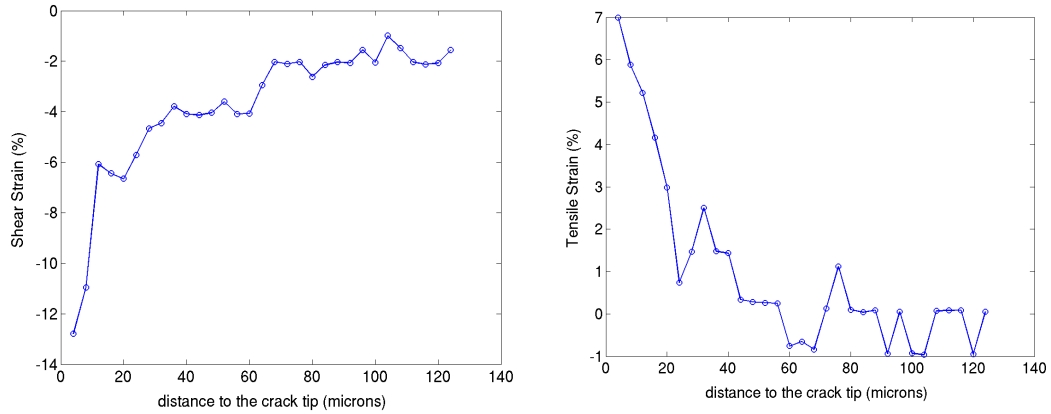

Figure 7. Shear (left) and tensile (right) strain range profiles measured along the ligament during the Mode II stage of the sequential cycle, for $\Delta K_I = \Delta K_{II}$.

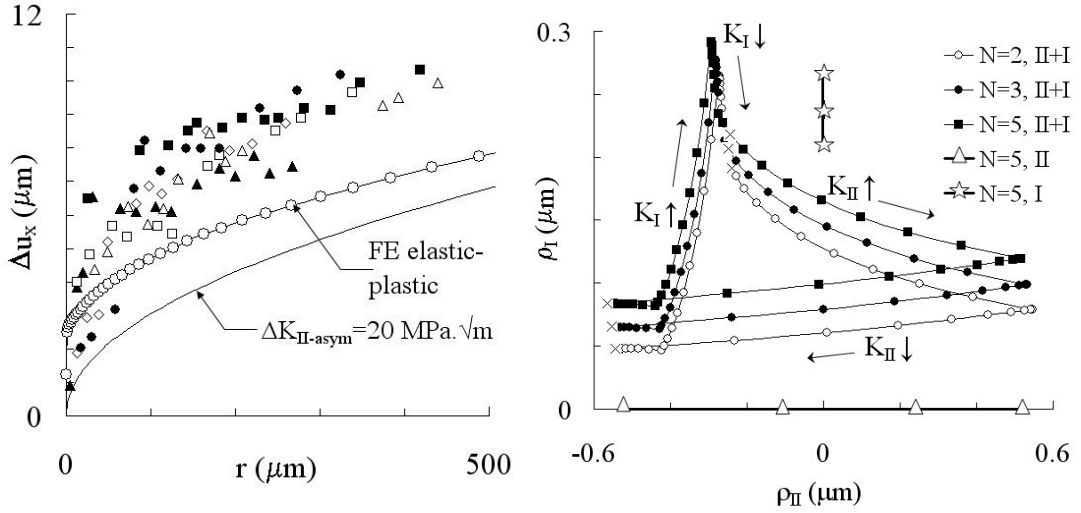

Figure 8. a) Sliding displacements measured during sequential Mode I /II and b)"plastic sliding and opening displacements" computed 250μm behind the crack tip.

Discussion

Residual stresses left just ahead of the crack by the Mode I cycle might explain the observation of Fig. 7, as illustrated by Fig. 9a, which shows a schematic 2D section of the elastic domain of the material translated by kinematic hardening during the Mode I plastic flow. During the subsequent cycle in Mode II, plastic flow will thus be easier (the vertical cord is smaller than the diameter) and, due to the normality of plastic flow, both tensile and shear plastic strains will be produced, instead of pure shear for an annealed metal. In addition, ratchetting will lead to the accumulation of tensile strain, since the sign of the axial strain produced by reversed shear loading will be the same as in the forward sense. A symmetrical mechanism (Fig. 9b) could lead to the accumulation of shear strain during the Mode I stage of the cycles.

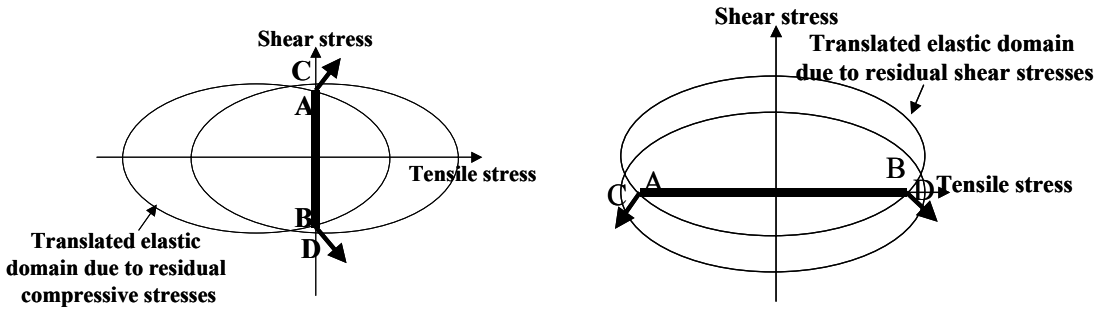

Figure 9. Schematic of plastic flow during the Mode II (left) or Mode I (right) part of a sequential test.

The fact that the measured sliding displacement profiles lie above the elastic asymptotic profile in sequential Mode I+II, is an additional evidence of the effective reduction of crack flanks friction by the Mode I cycle. Wong et al. also report an increase in the effective fraction of ΔK_{II} in sequential mixed mode compared to pure Mode II [1]. Figure 8b compares the evolution of the "plastic part of sliding and opening displacements" computed 250μm behind the crack tip during pure Mode I, pure Mode II and sequential Mode I +II, during the second, third and fifth cycles for $\Delta K_I = 0.75\Delta K_{II}$. Ratchetting in the crack opening clearly appears, consistently with Fig. 9a. This could also contribute to reduce crack flanks friction during the Mode II part of the cycle. A slight ratchetting towards negative shear displacements also appears, consistently with Fig. 9b. The fact that the measured sliding ranges are higher than the elastic-plastic displacement ranges has however still to be understood and F.E. simulations of crack growth through periodic node release will be undertaken towards this aim.

If, thanks to intermittent Mode I, $\Delta K_{II}^{effective}$ stays equal to $\Delta K_{II}^{nominal} = 20MPa\sqrt{m}$ instead of decreasing with the crack length, like in pure Mode II, this would explain the stability of the crack path for $\Delta K_I = 0.25\Delta K_{II}$, a case for which synergetic effects due to plasticity are not observed in terms of growth rate. Knowing $K_I(t)$, $K_{II}(t)$ for the main crack, and using the functions tabulated by Amestoy et al [2], the S.I.Fs on any potential infinitesimal branch crack in the direction θ, $k_1^*(t,\theta)$, $k_2^*(t,\theta)$ can be computed and their range other one cycle $\Delta k_1^*(\theta)$, $\Delta k_2^*(\theta)$ deduced. For the first part of the sequential test ($\Delta K_I = \Delta K_{II}$, Fig. 10a) Δk_1^* and Δk_2^* are both maximum for $\theta \approx 0°$ and no facet satisfies the "local symetry" criterion ($\Delta k_2^*=0$) so that coplanar growth is necessarily stable. For the fourth part of the sequential test ($\Delta K_I = 0.25\Delta K_{II}$, Fig. 10b) Δk_1^* is maximum ($12.3MPa\sqrt{m}$) and Δk_2^* minimum ($2.2MPa\sqrt{m}$) for $\theta \approx 75°$. The growth rate along this potential direction, computed from the Mode I data provided by Ascométal (the Mode II contribution is negligible) appears to be 3.4 times smaller than the coplanar growth rate during sequential mixed-mode loading. According to the maximum velocity criterion first proposed by Hourlier and Pineau [3], coplanar growth should thus be preferred.

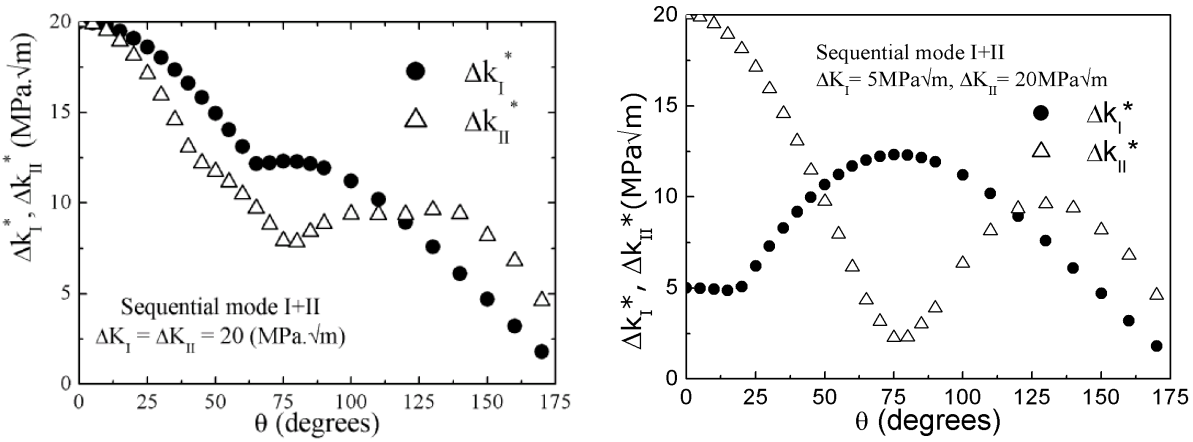

Figure 10. Mode I and Mode II SIFs on a branch crack as a function of its orientation.

CONCLUSIONS AND FINAL REMARKS

For a given ΔK_{II}, wear of asperities, ratchetting and plasticity at the crack tip are more important for R= 0 than for R= -1. This was shown by micro-grids distortions as well as F.E. simulations Similar crack growth rates seem however to result for a given nominal ΔK_{II}.

Under sequential mixed mode loading, coplanar growth seems stable (less friction, no deceleration). For a mixity ratio equal to 0.25, the contributions of each mode to the growth rate are simply added. For higher mixity ratios, a synergetic effect (due to residual stresses and normality of plastic flow giving rise to biaxial ratchetting) accelerates the crack growth.

The maximum growth rate criterion rationalises the crack path observed in such non-proportional loadings. Further research is however needed to investigate the influence of the loading path. Are effective S.I.Fs sufficient to describe crack growth rates under non-proportional loadings or do we need new loading path-dependent parameters?

Acknowledgements. This study was partly supported by Ascometal-CREAS.

REFERENCES

1. Wong, S.L., Bold, P.E., Brown, M.W. and Allen, R.J. (1996) *Wear* **191**, 45-53.
2. Amestoy, M., Bui, H.D. and Dang Van, K.(1979) C.R. Acad.Sci.Paris, B289, 99-102
3. Hourlier, F. and Pineau, A. (1981) In *Advances in fracture research*, Proc.5th Int.Conf.Fracture, Vol. 4, pp. 1841-49.